21st Australasian Fluid Mechanics Conference
Adelaide, Australia
10-13 December 2018

Effect of inflow conditions on the air-water flow properties in hydraulic jumps

L. Montano[1] and S. Felder[1]

[1]Water Research Laboratory, School of Civil and Environmental Engineering
UNSW Sydney, NSW 2052, Australia

Abstract

A hydraulic jump occurs in the transition from fast flows to slow flows. While extensive research has been conducted of air-water flow properties in hydraulic jumps with partially developed inflow conditions, only few studies have analysed the effect of the boundary layer development upstream of the hydraulic jump on the air-water flow features. Previous studies showed effects of the inflow condition on void fraction and bubble sizes. New experiments were conducted to extend the research of the effect of inflow conditions to a wider range of air-water flow properties. For hydraulic jumps with identical Froude and Reynolds numbers, but partially and fully developed inflow conditions, the comparative analysis of air-water flow properties highlighted an increase in void fraction, bubble count rate, and interfacial velocities in hydraulic jumps with fully developed inflow condition, while the chord sizes were comparatively smaller for the partially developed inflow condition.

Introduction

A hydraulic jump is a hydraulic phenomenon characterised by a rapid transition from supercritical to subcritical flows. Hydraulic jumps with inflow Froude numbers (Fr_1) above 4.5 are characterised by strong flow turbulence, air entrainment and energy dissipation [1,7]. Extensive research has been conducted of air entrainment in hydraulic jumps [e.g. 4,8,9,10]. Most experimental air-water flow studies were conducted under partially developed inflow conditions. However, in many practical applications, including in the stilling basin at the downstream end of a spillway, the flow is likely fully developed. A recent series of experiments by [11] showed a strong influence of the inflow conditions on the air entrainment characteristics in hydraulic jumps supporting earlier works by [9,10]. These studies [9,10,11] highlighted that hydraulic jumps with fully developed inflow conditions had larger void fractions and bubble sizes. This effect was linked to larger turbulence levels upstream of the hydraulic jump in fully developed inflows. While these studies provided some first insights into the importance of the inflow conditions upstream of hydraulic jumps, new experiments were conducted in the present study to test the effect of inflow conditions for a wider range of air-water flow properties including void fraction, bubble count rate, interfacial velocity and probability distribution functions of chord sizes. The present study was conducted for identical Froude and Reynolds (Re) numbers under partially and fully developed inflow conditions. The results showed an effect of inflow conditions on all tested air-water flow properties highlighting that the upstream inflow conditions must be taken into account in the characterisation of internal flow features of hydraulic jumps.

Experimental setup

New experiments were conducted in a long horizontal smooth channel of 0.6 m width and 40 m length at the Water Research Laboratory, UNSW Sydney. Figure 1 presents a sketch of the experimental facility including the definition of key parameters. At the upstream end of the channel, a sluice gate with a rounded upstream edge (Ø = 5 cm) provided uniform supercritical inflows upstream of the hydraulic jumps with depth (d_1). The longitudinal position of the hydraulic jump was controlled with a tail gate located at the downstream end of the channel. The discharge (Q) was supplied directly from Manly Dam and was controlled with an ABB® flow meter with an accuracy of ±0.4%. The flow profiles, boundary layer properties and inflow conditions were measured with a Pitot tube (Ø = 3 mm) at several cross sections downstream of the sluice gate. The air-water flow properties in channel centre line were measured with a self-developed double-tip conductivity probe with an inner electrode of Ø = 0.125 mm [5,6]. The longitudinal and transversal separation distance between the probe's leading and trailing tips were Δx = 7.9 mm and Δz = 1 mm respectively. A detailed sensitivity analysis of the effect of sampling time on the void fraction and bubble count rates in hydraulic jumps was conducted for a sampling rate of 20 kHz (not shown in this manuscript). The results identified minimum sampling times of 5 to 6 minutes close to the jump toe ($(x-x_1)/d_1 \leq 8$), and 4 minutes further downstream ($(x-x_1)/d_1 > 8$) to avoid large deviations in the air-water flow properties, where x is the distance from the sluice gate and x_1 is the jump toe position relative to the sluice gate. All present air-water flow measurements were therefore conducted for 5 and 4 minutes respectively.

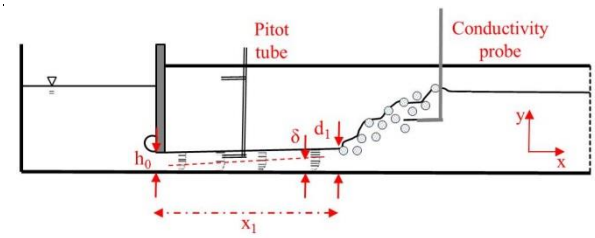

Figure 1. Experimental setup in the present study.

The present hydraulic jumps with fully and partially developed inflow conditions had identical Froude and Reynolds numbers of Fr_1 = 8.5 and Re = 7.5×10^4 corresponding to d_1 = 0.02 m and Q = 0.045 m^3/s. The same Froude and Reynolds numbers were achieved by adjustment of the gate opening (h_0). For the hydraulic jump with partially developed inflows (δ/d_1 = 50%), h_0 = 0.016 m and for the fully developed flow case (δ/d_1 > 100%), h_0 = 0.019 m.

Inflow conditions

The inflow conditions were identified in a series of experiments with flow rates 0.037 < Q < 0.058 m^3/s and gate openings 0.02 < h_0 < 0.04 m. At several cross sections downstream of the sluice gate, the time-averaged velocities (V) were measured with the Pitot tube. Figure 2 shows typical dimensionless velocity V/V_0 distributions as a function of the dimensionless elevation above channel bed y/h_0 at different dimensionless positions downstream of the sluice gate x/h_0 for one discharge and gate opening, where V_0 is the free-stream velocity. For the same flow rate and gate opening, the magnitude of the velocities decreased with increasing distance downstream of the sluice gate as a result of the increase in the flow depth in downstream direction. Similar velocity

distributions were observed for all discharges and gate openings. At all cross-sections, the boundary layer thickness (δ) was determined as the elevation where the local velocity was 99% of the free-stream velocity. The present estimates of the turbulent boundary layer growth rate were in close agreement with the empirical equation by [12]:

$$\frac{\delta}{h_0} = 0.0366 \times \left(\frac{x}{h_0}\right)^{4/5} \quad (1)$$

The values of δ are also added in Figure 2 showing the close agreement between the present data and Equation (1).

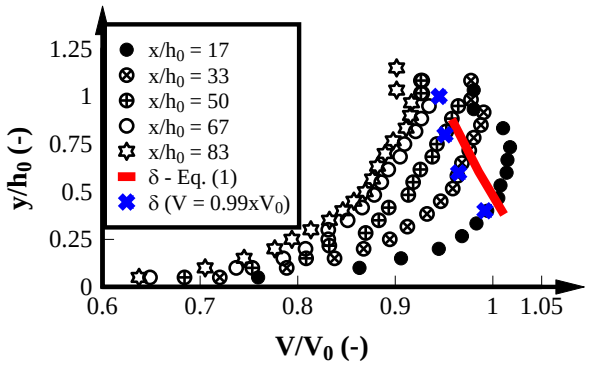

Figure 2. Velocity distributions at several cross-sections downstream of the sluice gate: Q = 0.058 m^3/s, h_0 = 0.03 m; Comparison with Equation (1) and estimated boundary layer thickness δ

Comparison of flow features of hydraulic jumps with different inflow conditions

Visual observations

The hydraulic jumps were turbulent and unstable for fully and partially developed inflow conditions. Figure 3 presents the hydraulic jumps with fully and partially developed inflow conditions respectively and the cross-sectional areas measured with the conductivity probe as reference points.

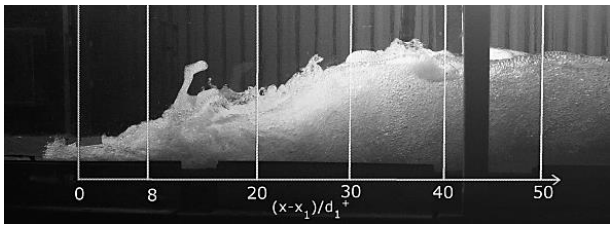

(a) Hydraulic jump with fully developed inflow conditions.

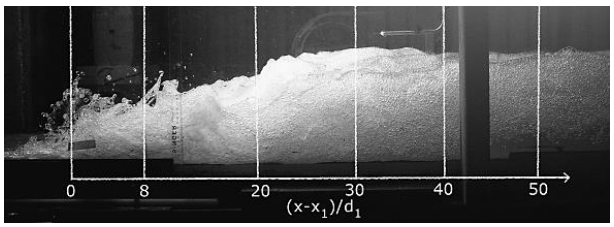

(b) Hydraulic jump with partially developed inflow conditions

Figure 3. Visual observations of effects of inflow conditions on the air-water flow features in hydraulic jumps in the present study: Fr_1 = 8.5, Re = 7.5×10^4.

The visual observations showed similar aeration, turbulence and free-surface features for both hydraulic jump types. Within the jump roller, for $(x-x_1)/d_1 \leq 40$, large air entrainment was observed represented by the white colour (Figure 3). Within this flow region, little differences were observed between the two hydraulic jump types. At the downstream end, for $(x-x_1)/d_1 = 50$, larger whitish colour was observed in the hydraulic jump with partially developed inflow conditions (Figure 3b) while the jump with fully developed inflow conditions showed a larger clear water layer close to the channel bed suggesting an upwards directed jump roller in the downstream section of the hydraulic jump. The hydraulic jump with partially developed inflow conditions was characterised by larger jump toe instabilities linked with larger sensitivity to small variations in the tail gate position downstream.

Void fraction distributions

Figure 4 presents a comparison of the void fraction (C) distributions for fully and partially developed inflow conditions as a function of the dimensionless elevation above channel bed y/d_1. For all cross-sections, the void fraction distributions followed a typical shape with two marked regions, i.e. a shear region or lower region characterised by the advective transport of bubbles and the recirculation or upper region characterised by splashes, air-water flux and foam [3,4,8]. The comparison of C was conducted at the same dimensionless locations along the hydraulic jumps $(x-x_1)/d_1$. The hydraulic jump with fully developed inflow conditions showed larger void fractions in the shear region at all cross-sections. The present results were consistent with the findings of [11]. The maximum void fractions in the shear region (C_{max}) under fully developed inflow conditions were more than 30% larger than C_{max} in partially developed inflow conditions suggesting stronger advective transport of bubbles for fully developed inflow conditions when the free-surface upstream of the hydraulic jump was affected by the turbulent boundary layer. Apart from $(x-x_1)/d_1 = 8$, the void fraction profile of the partially developed inflow case was consistently lower in the recirculation region suggesting lower free-surface elevations.

The void fraction profiles were compared with the theoretical advective diffusion equation for air bubbles in hydraulic jumps which was established by [2,3,8] in the shear region:

$$C = C_{max} \times exp\left(-\frac{1}{4 \times D^{\#}} \times \frac{\left(\frac{y - Y_{C_{max}}}{d_1}\right)^2}{\left(\frac{x - x_1}{d_1}\right)}\right)$$

for $0 < y < y^*$ (2)

and recirculation region:

$$C = \frac{1}{2} \times \left(1 + \text{erf}\left(\frac{y - Y_{50}}{2 \times \sqrt{\frac{D^* \times (x - x_1)}{V_1}}}\right)\right) \quad \text{for } y > y^* \quad (3)$$

where $D^{\#} = D_t/(V_1 \times d_1)$, D_t is the diffusivity in the shear region, V_1 is the inflow velocity, Y_{Cmax} is the elevation at C_{max}, D^* is the dimensionless diffusivity coefficient in the recirculation region, y* is the upper limit of the shear region and Y_{50} is the elevation with C = 0.5. All void fraction distributions presented good agreement with Equations (2) and (3) independent of the inflow conditions with slight deviations in the transition between the shear and recirculation regions (Figure 4). The differences were more pronounced for hydraulic jumps with fully developed inflow conditions. The experimental void fraction distributions were also compared with previous studies and close similarities were identified

between the experimental data collected by [11,12] for comparable Froude and Reynolds numbers (not shown).

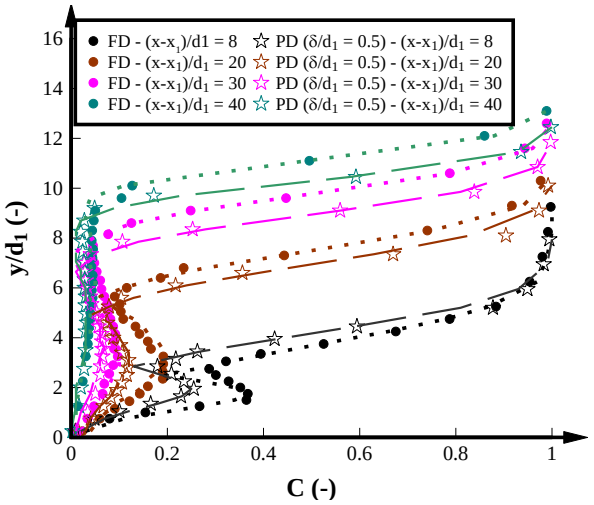

Figure 4. Comparison of void fraction distributions for fully and partially developed inflow conditions at several cross sections along the hydraulic jump: Fr_1 = 8.5, Re = $7.5x10^4$. Comparison with the advective diffusion equation for air bubbles in hydraulic jumps (Equations (2) and (3)): Dotted line = fully developed inflow conditions; Dashed lines = partially developed inflow conditions.

Bubble count rate

The bubble count rate (F) represents the average number of bubbles per second recorded by the conductivity probe. Figure 5 presents bubble count rate distributions for partially and fully developed inflow conditions at different cross-sections along the hydraulic jump. For all cross-sections and independent of the inflow conditions, the bubble count rate distributions showed typical shapes with one peak in the shear region and a second peak in the recirculation region. Large differences were observed in the bubble count rate distributions between fully and partially developed inflow conditions in both the shear and recirculation regions with larger bubble count rates in both flow regions for the fully developed hydraulic jump. The maximum bubble count rate in the shear region for the fully developed case was about 30% larger compared to the hydraulic jump with partially developed inflow conditions. Similar differences were observed in the maximum bubble count rate in the recirculation region with larger number of entrained air bubbles for the fully developed hydraulic jump. At the downstream end of the roller, the hydraulic jump with fully developed inflow conditions showed a faster decrease in bubble count rate in the shear region while the peak in the recirculation region increased. These results were in agreement with the visual observations of lesser air entrainment close to the channel bed for fully developed hydraulic jumps (Figure 3). Despite the lesser number of bubbles at the downstream end of the jump in the shear region, the void fraction distribution was still larger for fully developed hydraulic jumps. A decrease in the number of bubbles with larger void fraction corresponded to larger bubble sizes which provoked bubble rise due to buoyancy and larger number of bubbles in the recirculation region for fully developed hydraulic jumps.

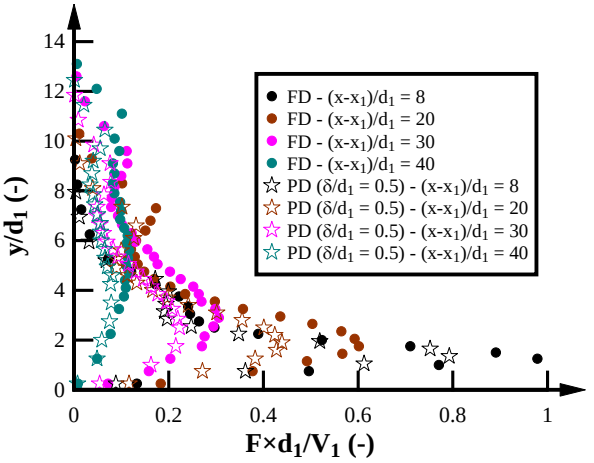

Figure 5. Comparison of bubble count rates distributions for fully and partially developed inflow conditions at different cross-sections along the hydraulic jump: Fr_1 = 8.5, Re = $7.5x10^4$.

Interfacial velocity

The interfacial velocity (V*) was estimated as V* = Δx/T where Δx is the longitudinal separation distance between the tips of the probe and T is the average travel time of the air-water flow. Figure 6 shows the dimensionless interfacial velocity distributions as a function of y/d_1 at two different cross-sections. Close to the jump toe ($(x-x_1)/d_1 \leq 20$), the hydraulic jumps with partially developed inflow conditions had lower interfacial velocities in the shear region while negative velocities of similar magnitude were identified in the recirculation region (Figure 6a). Further downstream, ($(x-x_1)/d_1 > 20$, the interfacial velocity distributions were similar for the hydraulic jumps with fully and partially developed inflow conditions (Figure 6b). The result suggested that close to the jump toe in fully developed inflow conditions, the advective transport of bubbles into the jump may occur faster related with the larger inflow turbulent levels close to the free-surface.

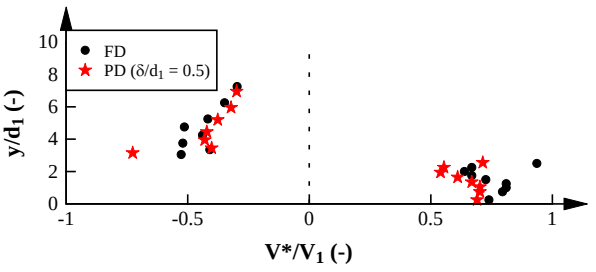

(a) $(x-x_1)/d_1$ = 8

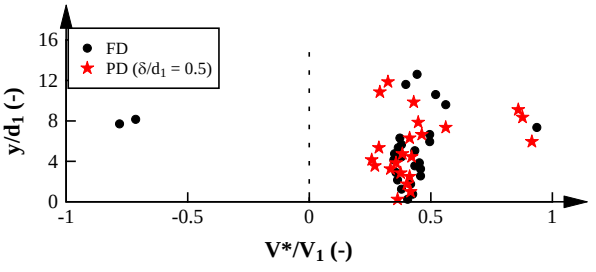

(b) $(x-x_1)/d_1$ = 30

Figure 6. Comparison of the interfacial velocity distributions for fully and partially developed inflow conditions at different cross-sections along the hydraulic jump:Fr_1 = 8.5, Re = $7.5x10^4$.

Chord times

The chord times are defined as the time between interface changes (air-to-water or water-to-air). While they do not represent the sizes of the air bubbles and water droplets, the chord times characterise the sizes of the air and water entities. Figure 7 presents the probability distribution functions (PDF) of the air bubble chord times at C_{max} for hydraulic jumps with fully and partially developed inflow conditions. For both hydraulic jump types and at different cross-sections, the PDF of the chord sizes showed a larger percentage of small bubbles. The characteristic peak in bubble sizes decreased with increasing distance from the jump toe suggesting a more even distribution of bubble sizes towards the downstream end of the hydraulic jumps.

No significant differences were observed in the PDF between partially and fully developed inflow conditions at C_{max}. The comparison of the large bubble times showed that the hydraulic jump with fully developed inflow conditions presented comparatively larger bubble sizes. This result was in agreement with visual observations of larger bubbles close to the surface for the hydraulic jump with fully developed inflow conditions.

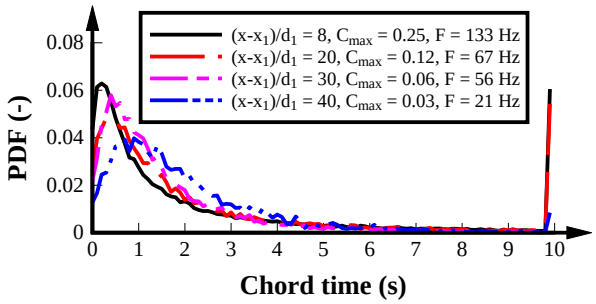

(a) Hydraulic jump with fully developed inflow conditions.

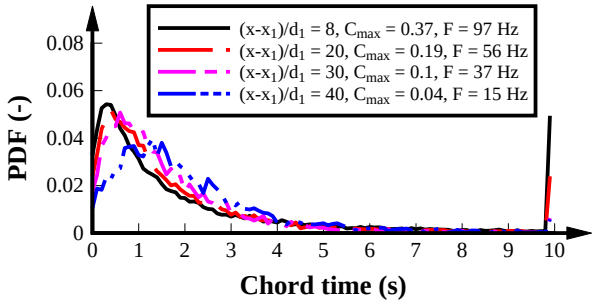

(b) Hydraulic jump with partially developed inflow conditions

Figure 7. PDF of the air bubble chord times for C_{max} at different cross-sections along the hydraulic jump.

Conclusions

The air-water flow properties in a hydraulic jump with Fr_1 = 8.5 and Re = 7.5×10^4 with partially and fully developed inflow conditions were investigated. Similar visual observations were identified for both jump types with slightly larger flow aeration at the downstream end for the hydraulic jump with partially developed inflow conditions. Larger jump toe instabilities were also observed for the partially developed inflow case. The hydraulic jump with fully developed inflow conditions showed larger void fractions in the shear region and higher void fraction profiles in the recirculation region. Both hydraulic jump types were closely matched by the advective diffusion equations. The bubble count rate distributions were consistently larger in the fully developed hydraulic jump for both shear and recirculation regions. The interfacial velocity distributions were almost the same for both hydraulic jumps with slightly larger velocities close to the jump toe for the fully developed inflow conditions. At the C_{max} position, the fully developed hydraulic jump was characterised by larger bubble sizes in comparison with the partially developed jump. This result was consistent with the larger aeration and decrease in the number of bubbles at the downstream end of the hydraulic jump. Overall, the fully developed hydraulic jump showed larger aeration, larger number of bubbles, larger bubble sizes and larger velocities confirming a strong effect of the inflow conditions on the air-water flow properties in hydraulic jumps. The present study highlighted that the inflow conditions upstream of a hydraulic jump must be taken into consideration.

Acknowledgments

The authors thank Rob Jenkins (WRL, UNSW Sydney) for his technical assistance with building the sluice gate. They thank A/Prof Ron Cox (WRL, UNSW Sydney) for his advice.

References

[1] Bradley, J.N. & Peterka, A.J., Hydraulic Design of Stilling Basins, *J. Hydr. Eng. Div-ASCE*, 5, 1957.

[2] Brattberg, T., Chanson, H. & Toombes, L. Experimental Investigations of Free-Surface Aeration in the Developing Flow of Two-Dimensional Water Jets, *Trans. ASME*, 120, 1998, 738-744.

[3] Chanson, H., Air entrainment in two-dimensional turbulent shear flows with partially developed inflow conditions, *Int. J. Multiphase Flow*, 21(6), 1995, 1107-1121.

[4] Chanson, H. & Brattberg, T., Experimental study of the air-water shear flow in a hydraulic jump, *Int. J. Multiphase Flow*, 26(4), 2000, 583-607.

[5] Felder, S. & Chanson, H., Air-Water Flow Patterns of Hydraulic Jumps on Uniform Beds Macroroughness, *J. Hydraul. Eng.*, 144(3), 2018, 1-12.

[6] Felder, S. & Pfister, M., Comparative analyses of phase-detective intrusive probes in high-velocity air-water flows, *Int. J. Multiphase Flow*, 90, 2017, 88-101.

[7] Hager, W.H., *Energy Dissipators and Hydraulic Jump*, Kluwer Academic Publishers, 1992.

[8] Murzyn, F., Mouaze, D. & Chaplin, J.R., Optical fibre probe measurements of bubbly flow in hydraulic jumps, *Int. J. Multiphase Flow*, 31, 2005, 141-154.

[9] Resch, F.J. & Leutheusser, H.J., Le ressaut hydraulique: mesures de turbulence dans la región diphasique, *La Houille Blanche*, 4, 1972, 279-293.

[10] Resch, F.J., Leutheusser, H.J. & Alemu, S., Bubbly two-phase flow in hydraulic jump, *J. Hydr. Eng. Div.-ASCE*, 100(1), 1974, 137-149.

[11] Takahashi, M. & Ohtsu, I., Effects of inflows on air entrainment in hydraulic jumps below a gate, *J. Hydraul. Res.*, 55(2), 2017, 259-268.

[12] Wang, H., Turbulence and air entrainment in hydraulic jumps, *Ph.D. thesis*, The University of Queensland, Australia, 2014.